Louisiana State University
LSU Digital Commons

Faculty Publications

Department of Oceanography & Coastal Sciences

2021

Marginal warming associated with a COVID-19 quarantine and the implications for disease transmission

P. W. Miller

C. Reesman

M. K. Grossman

S. A. Nelson

V. Liu

See next page for additional authors

Follow this and additional works at: https://digitalcommons.lsu.edu/oceanography_coastal_pubs

 Part of the Environmental Sciences Commons

Authors

P. W. Miller, C. Reesman, M. K. Grossman, S. A. Nelson, V. Liu, and P. Wang

Science of the Total Environment 780 (2021) 146579

Contents lists available at ScienceDirect

Science of the Total Environment

journal homepage: www.elsevier.com/locate/scitotenv

Marginal warming associated with a COVID-19 quarantine and the implications for disease transmission

P.W. Miller [a,*], C. Reesman [a], M.K. Grossman [b], S.A. Nelson [a], V. Liu [a], P. Wang [c]

[a] Coastal Meteorology (COMET) Lab, Department of Oceanography and Coastal Sciences, Louisiana State University, Baton Rouge, LA, USA
[b] Geospatial Research, Analysis and Services Program, Division of Toxicology and Human Health Sciences, ATSDR, USA
[c] Department of Oceanography and Coastal Sciences, Louisiana State University, Baton Rouge, LA 70803, USA

HIGHLIGHTS

- Urban aerosol fraction decreased from 27.1% to 17.5% during China's COVID response.
- Reduced COVID-19 particulate loads yielded +0.2 °C warming across east-central China.
- Air quality-related warming may marginally retard disease transmission during lockdowns.

GRAPHICAL ABSTRACT

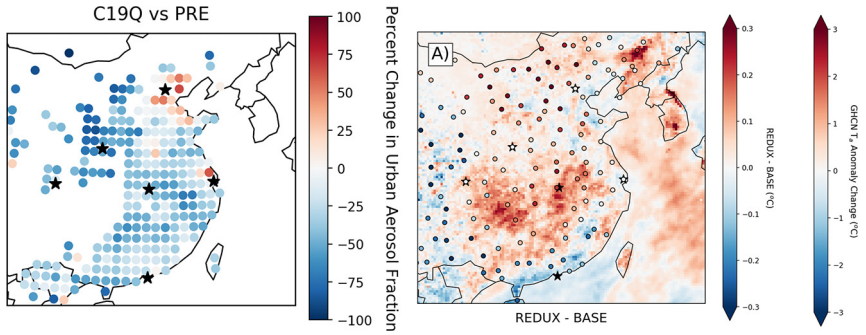

ARTICLE INFO

Article history:
Received 15 January 2021
Received in revised form 15 March 2021
Accepted 15 March 2021
Available online 19 March 2021

Editor: Scott Sheridan

Keywords:
COVID-19
Quarantine
Aerosols
Temperature
Transmission

ABSTRACT

During January–February 2020, parts of China faced restricted mobility under COVID-19 quarantines, which have been associated with improved air quality. Because particulate pollutants scatter, diffuse, and absorb incoming solar radiation, a net negative radiative forcing, decreased air pollution can yield surface warming. As such, this study (1) documents the evolution of China's January–February 2020 air temperature and concurrent particulate changes; (2) determines the temperature response related to reduced particulates during the COVID-19 quarantine (C19Q); and (3) discusses the conceptual implications for temperature-dependent disease transmission. C19Q particulate evolution is monitored using satellite analyses, and concurrent temperature anomalies are diagnosed using surface stations and *Aqua* AIRS imagery. Meanwhile, two WRF-Chem simulations are forced by normal emissions and the satellite-based urban aerosol changes, respectively. Urban aerosols decreased from 27.1% of pre-C19Q aerosols to only 17.5% during C19Q. WRF-Chem resolved ~0.2 °C warming across east-central China, that represented a minor, though statistically significant contribution to C19Q temperature anomalies. The largest area of warming is concentrated south of Chengdu and Wuhan where temperatures increased between +0.2–0.3 °C. The results of this study are important for understanding the anthropogenic forcing on regional meteorology. Epidemiologically, the marginal, yet persistent, warming during C19Q may retard temperature-dependent disease transmission, possibly including SARS-CoV-2.

© 2021 Elsevier B.V. All rights reserved.

1. Introduction

During February 2020, large areas of east China were sequestered by COVID-19 containment measures. Though the most concentrated early outbreak occurred in Wuhan, other areas of eastern China also faced COVID-19 spread, and mobility restrictions were extended well beyond

* Corresponding author.
E-mail address: pmiller1@lsu.edu (P.W. Miller).

https://doi.org/10.1016/j.scitotenv.2021.146579
0048-9697/© 2021 Elsevier B.V. All rights reserved.

the early epicenter. As commuter traffic (Lian et al., 2020) and industrial activity declined, satellite-based concentrations of nitrogen dioxide (NO_2), a secondary inorganic aerosol typically associated with high-temperature combustion, fell by 48% compared to the 20-day period immediately preceding the quarantines (Liu et al., 2020b). Similarly, in-situ measurements of NO_2 indicated reductions of 60% over north China (Shi and Brasseur, 2020), which were compounded by the annually reduced emissions during the Chinese New Year (e.g., J. T. Lin and McElroy, 2011) on 25 January 2020. As the world has continued grapple with COVID-19, air quality improvements have now been documented in a number of cities and regions globally, including Seoul (Seo et al., 2020), Tuscany (Donzelli et al., 2020), Sydney, Dehli, Johannesburg, Moscow, and others (Fu et al., 2020).

While NO_2 concentrations have important public health implications, its presence is also associated with other harmful air pollutants. For instance, concentrations of fine particulate matter (aerodynamic diameters <2.5 μm; $PM_{2.5}$), also emitted from human activity, declined by 35% over north China coincident with the NO_2 reductions (Shi and Brasseur, 2020), though similar reductions were not observed in U.S. cities (Bujin et al., 2020; Jia et al., 2020). However, the secondary formation of fine particulates in the atmosphere as a result of chemical processes (Kroll et al., 2020) led to the paradoxical persistence of haze events in Beijing-Tianjin (e.g., Huang et al., 2020a; Wang et al., 2020a; Zhao et al., 2020) and Shanghai (e.g., Chang et al., 2020) despite reduced emissions. Changes in the amount of particulate matter, also termed aerosols, in the atmosphere is significant from a meteorological perspective. As incoming solar radiation passes through the atmosphere, aerosols can reflect, scatter, and absorb energy before the radiation reaches the earth's surface. These radiative interactions, termed the aerosol direct effect, produce a net dimming of solar radiation (IPCC, 2014), which can in turn reduce surface air temperature (e.g., Forster et al., 2020; Jin et al., 2010).

In the months following the onset of the pandemic, modeling studies have identified sub-degree warming driven by COVID-19-related aerosol reductions over China, ranging from +0.13 °C (Gettelman et al., 2020), +0.05–0.15 °C (Yang et al., 2020), and +0.30 °C (Diffenbaugh et al., 2020). Simultaneously, numerous epidemiological analyses have examined the relationship between warmer temperatures and reduced COVID-19 transmission, producing hotly debated and conflicting conclusions (e.g., Huang et al., 2020c; Huang et al., 2020b; Jamil et al., 2020; Liu et al., 2020c; Lolli et al., 2020; Pan et al., 2021; Yao et al., 2020; Zhang et al., 2020). Regardless, the transmission of numerous existing (and likely future) communicable diseases *is* temperature-dependent (NRC, 2001), including other coronaviruses (Kissler et al., 2020). Therefore, the aforementioned lockdown-warming research implies a potential lockdown-warming-transmission feedback that has implications for public health well beyond the current pandemic.

Though several studies have examined how regional meteorology influenced COVID-19 air quality changes in east China (e.g., Su et al., 2020; Sulaymon et al., 2021), fewer have contemplated the question from the other direction, whereby meteorological conditions are analyzed as a function of air quality based on the aerosol direct effect. Consequently, this study investigates (1) did air quality changes during the COVID-19 quarantine influence the observed temperature patterns; and (2) if so, what are the implications of lockdown-driven warming for temperature-dependent disease transmission? Though air pollution is hypothesized to be one variable influencing the COVID-19 temperature patterns in China, this study is not focused on the region's air quality in and of itself. Instead, it is most centered on the meteorological effects of the altered the radiative transfer. Remotely sensed and in-situ measurements are employed to characterize meteorological conditions before and during the quarantine, while concurrent changes in anthropogenic particulate concentrations are inferred from the *NOAA-20* satellite and used to force a regional weather model. The effect on surface temperature is quantified, compared to observed patterns, and then discussed in terms of the COVID-19 reproductive number (R), a measure of a disease's transmission potential.

2. Data and methods

2.1. Observational analysis

Remotely sensed daily surface air temperatures were accessed for 1 January – 1 March 2003–2020 from the Atmospheric Infrared Sounder (AIRS) instrument onboard the NASA *Aqua* satellite. Launched in May 2002, *Aqua* follows a global, sun-synchronous orbit with AIRS temperatures designed to achieve a 1 K accuracy in the lower troposphere under clear and partly cloudy conditions (Aumann et al., 2003). Because surface temperatures increase seasonally during the two-month retrieval period, daily anomalies were computed for each pixel using the 18-yr period of record. The analysis was separated into two periods, 1–22 January 2020 and 23 January – 1 March 2020 to characterize the evolution of aerosol concentrations and temperature during the implementation of the quarantines. The latter period represents the timespan when mobility restrictions were strictest (Sulaymon et al., 2021), and will hereafter be referenced as the C19Q period, whereas the pre-C19Q period (1–22 January 2020) will be termed PRE. Though mobility remained restricted in some locations beyond 1 March 2020 (Sulaymon et al., 2021), this study focuses on the period when containment was most prevalent. Meanwhile, the Global Historical Climatology Network (GHCN) (Menne et al., 2012a; Menne et al., 2012b) supplied in-situ daily mean temperature (T_{AVG}) observations for 153 active GHCN sites in China east of 90°E with at least 50 years of records. The same PRE and C19Q anomalies were calculated for the GHCN T_{AVG} as the AIRS observations. Large-scale lower-tropospheric patterns were visualized with the ERA5 global atmospheric reanalysis (Hersbach et al., 2020).

Aerosol optical depth (AOD) measurements were retrieved from *Terra*'s Moderate Resolution Imaging Spectroradiometer (MODIS) (2003−2020) and *NOAA-20*'s Visible Infrared Imaging Radiometer Suite (VIIRS). While *Terra* MODIS AOD possesses a longer period of record, Level 2 *NOAA-20* VIIRS AOD data contain the diagnosis of an intermediate aerosol model that classifies aerosols in each pixel as either predominantly oceanic, dust, generic, urban, or heavy smoke (Laszlo and Liu, 2016). For each 0.10° pixel over east China, the fraction of all PRE retrievals classified as "urban" was computed, and this process was repeated for C19Q. For instance, if a VIIRS pixel had 10 quality retrievals during PRE, and they were composed of four urban-, two smoke-, two dust-, and two oceanic-dominant days, then that pixel would receive a 40% PRE urban aerosol fraction. The change in urban aerosol fraction between the C19Q and PRE periods was determined and expressed as a percent change (i.e., decrease from 30% PRE urban aerosol retrievals to 15% during C19Q would correspond to a 50% reduction). Because some areas of the domain experience a low frequency of urban aerosols under normal circumstances or experienced a low number of quality retrievals (i.e., cloud contamination) in early 2020, percent increases/decreases could vary wildly (i.e., increase from 2% PRE urban aerosol retrievals to 6% during C19Q would correspond to a 200% increase). Thus, the analysis was coarsened to 1.0° resolution, and the percent change in urban aerosol fraction was only computed if the PRE fraction was at least 13.9%, the median value across the domain.

2.2. Modeling experiment

To characterize the relationship between urban aerosol changes and the coincident warmth, the Weather Research and Forecasting (WRF) model (Skamarock and Klemp, 2008) coupled with chemistry (WRF-Chem) (Grell et al., 2005) was initialized at 24-km grid spacing over an East Asia domain similar to other WRF-Chem work in China (Fig. 1) (e.g., Y. Gao et al., 2014; Zhang et al., 2015b) with anthropogenic emissions from the RETRO/EDGAR database (Crippa et al., 2018). Emissions from biogenic and wildfire were assumed unchanged and not included in this simulation since the anthropogenic aerosols were the focus of this study. The experiment was comprised of two simulations: (1) a

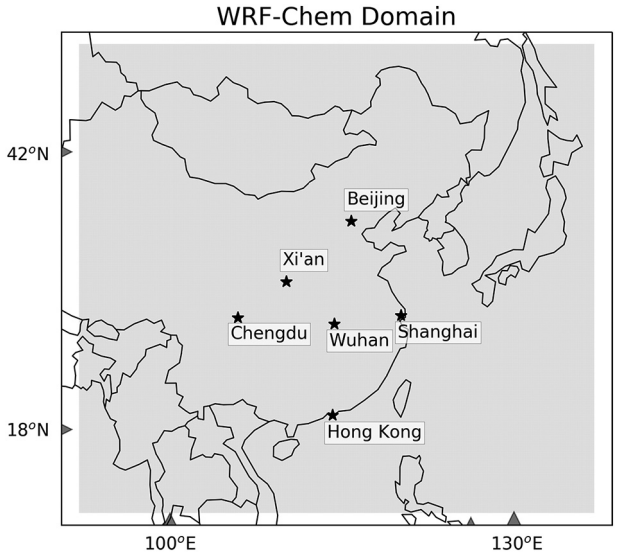

Fig. 1. WRF-Chem model domain. The six cities plotted above are also represented on all subsequent maps as reference points.

baseline scenario with unadjusted RETRO/EDGAR anthropogenic emissions (BASE) and (2) a C19Q scenario, with emissions adjusted using the change in urban aerosol fraction identified during the *NOAA-20* VIIRS analysis (REDUX). This technique deviates from other COVID-19 climate simulations that employ wholesale emissions removal (Diffenbaugh et al., 2020) or national/provincial-scale emissions adjustments in a global model (Forster et al., 2020; Gettelman et al., 2020; Yang et al., 2020). Table 1 lists the physical parameterizations and boundary condition dataset applied to the simulations which both employ the Regional Atmospheric Chemistry Mechanism (RACM) gas-phase chemistry model (Stockwell et al., 1997) coupled with the Georgia Tech/Goddard Global Ozone Chemistry Aerosol Radiation and Transport (GOCART) aerosol scheme (Ginoux et al., 2001). Four preliminary simulations using different of boundary layer schemes and boundary condition datasets were tested to ensure the physics in Table 1 yielded representative conditions.

Each simulation was initialized on 15 January 2020, and the emissions reduction is enforced at 0000 UTC 22 January 2020, near the start of China's Lunar New Year, as guided by an analysis of NO_2 measurements from the *Aura* OMI (Liu et al., 2020b) as well as air quality observations in Wuhan (Sulaymon et al., 2021). Discarding the first seven days as spin-up time, the analysis period begins on 23 January 2020. WRF-Chem fields were written to disk every six hours (00, 06, 12, and 18 UTC) corresponding to 8 AM/PM and 2 AM/PM Beijing local time. The change in aerosol-related temperature for the C19Q period was determined by subtracting the BASE T_{AVG} from the REDUX T_{AVG}.

Table 1
WRF-Chem physics settings applied to the simulations.

Physical parameterization	Scheme
Boundary conditions	GFS analysis
Microphysics	WSM 5-class
Cumulus	Grell 3D
Boundary layer	YSU
Land surface	Noah LSM
Surface layer	MM5 Monin-Obukhov
Shortwave radiation	RRTMG
Longwave radiation	RRTMG
Chemistry	GOCART coupled with RACM-KPP
Dust	GOCART-AWFA

2.3. Limitations

The methodological decisions described above are advantageous given this study's focus on regional meteorology but may be undesirable from an air quality monitoring perspective. For instance, the GOCART aerosol scheme coupled to the RACM chemistry model does not resolve the formation of secondary particulates (sulfates, nitrates, ammonium, secondary organic aerosols, etc.), which can be significant sources of $PM_{2.5}$ during winter haze (Huang et al., 2014). To accurately model secondary particulate formation, COVID-19 emissions changes in all precursor gases would need to be assimilated into a sophisticated chemistry and aerosol scheme, which might hopefully reproduce the satellite-observed changes we present in Section 3.2. Though post-COVID emissions inventories are available (Forster et al., 2020), they follow political boundaries and do not permit the same granularity as the VIIRS-based analysis.

Instead, the change in VIIRS urban aerosol fraction, which represents the net change in primary and secondary aerosol concentrations, can be used to initialize a simpler, faster scheme that does not attempt to resolve secondary particulate formation (i.e., GOCART). Thus, secondary particulates are implicitly modified by adjusting the PM primary emissions with the VIIRS analysis. The increases/decreases in urban aerosols are thus passed into WRF-Chem by altering emissions of the two particulate modes, $PM_{2.5}$ and PM_{10} (aerodynamic diameters <10 μm), which is sufficient for capturing the radiative forcing and its effect on temperature targeted by this study. While this approach strategically avoids the task of validating WRF-Chem's precursor gas and PM concentrations, it also has a drawback. Because temperature has a complicated, nonlinear relationship with secondary particulate formation (e.g., Kroll et al., 2020), the altered meteorological conditions which WRF-Chem is trying to characterize may contribute to the aerosol changes used to initialize it (Sheehan and Bowman, 2001). Given the complexity between the temperature-secondary PM relationship, this limitation can only be acknowledged and not quantified without further work.

3. Results

3.1. Observed temperature changes

AIRS data show that PRE temperature anomalies exceeded +3 °C over northeast China and ranged from +1–3 °C along the Yangtze River valley between Wuhan and Shanghai (Fig. 2a) with warm anomalies evident across southeast China as well. The C19Q period remained warmer-than-average over northeast China, though not to the same the extent as PRE (Fig. 2b). In contrast, southern China, experienced a much greater temperature transition, with negative surface temperature anomalies manifesting in this area during C19Q. Comparing the C19Q to PRE anomalies (Fig. 2c), relative warming during the C19Q period was concentrated in the eastern coastal plain where NO_2 decreases were most dramatic as determined by previous analyses (Liu et al., 2020b). The area of temperature anomaly increases qualitatively aligns with the region of AOD anomaly decreases during the C19Q period as determined by the *Terra* MODIS measurements (Fig. 2d).

Fig. 3 shows the same computation in Fig. 2c but for the GHCN surface stations. These in-situ observations indicate that C19Q anomalies increased beyond the region identified by the AIRS analysis in Fig. 2c. According to the GHCN, relative warming was more expansive with strong anomaly increases (+3 °C) located along the Mongolian border and moderate increases (+1–2 °C) extending further south into Hunan province. The longer, >50-yr period of record for the GHCN stations as opposed to the 18-yr AIRS dataset may alter the value of the 2020 anomalies for both the PRE and C19Q periods.

Though the region that experienced T_{AVG} anomaly increases from PRE to C19Q visually resembles the reduced AOD footprint (Fig. 2c–d), the correspondence may be a reflection of synoptic-scale influences. PRE was characterized by strong 850-hPa temperature anomalies,

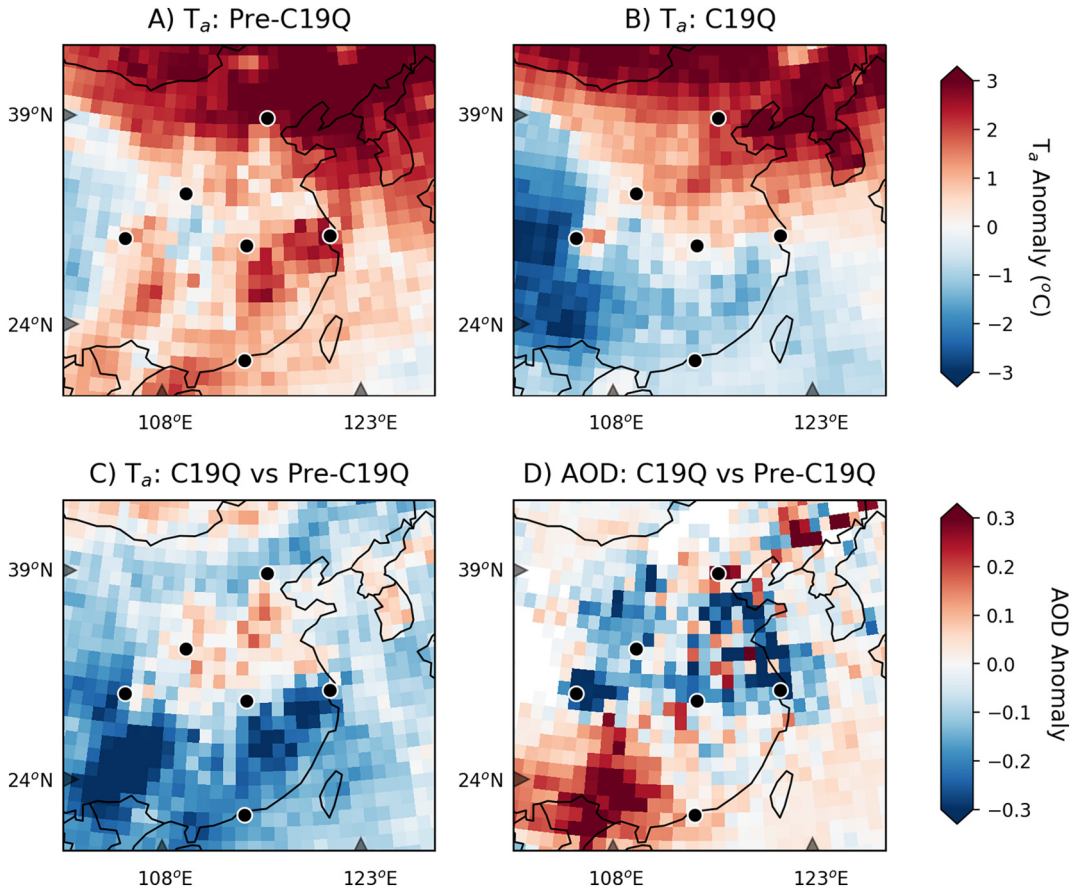

Fig. 2. *Aqua* AIRS mean T_{AVG} anomaly for the (A) PRE and (B) C19Q periods. The change in temperature anomaly between the two timespans (i.e., C19Q minus PRE) is shown in (C). The warming footprint is compared against the coincident change in *Terra* MODIS AOD anomaly (D), calculated in the same manner as the surface temperature comparison in (C). Both temperature and AOD anomalies were calculated with respect to the 2003–2020 AIRS period of record.

relative to the 1979–2020 mean (Fig. 4a). The positive anomalies occupy most of east China, with only a small pocket of slight cool anomalies in between Wuhan and Xi'an. Additionally, the footprint of warmer-than-average PRE 850-hPa temperatures closely mirror the areas of high surface temperature anomalies detected by AIRS (Fig. 2a). Meanwhile, C19Q was characterized by a much broader ridging pattern over Siberia that would have favored warmer-than-average conditions across most of Asia, including east China (Fig. 4b).

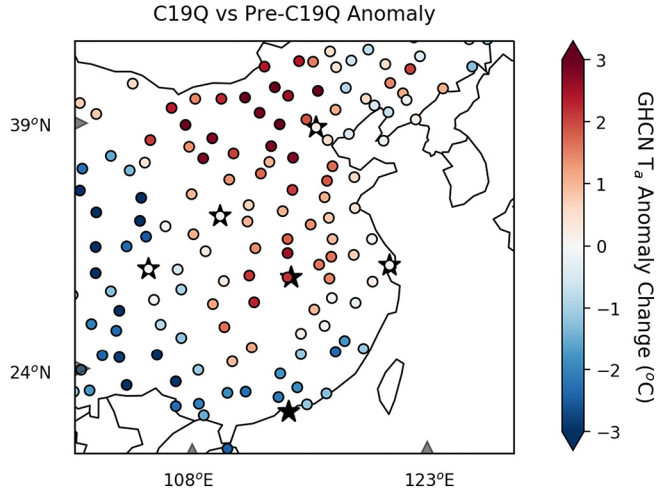

Fig. 3. Change in the T_{AVG} anomaly between the C19Q and PRE periods as measured at GHCN stations in east China with at least 50 years of data. Anomalies for each period were computed relative to each station's >50-yr period of record. The change in T_{AVG} anomaly represents the difference between C19Q and PRE anomalies.

Though much of east China also experienced warmer-than-average C19Q 850-hPa temperatures, the magnitude of the anomaly was smaller during C19Q for southern and northeast China. The small area of PRE cool anomalies transitions to a warm anomaly during C19Q. Fig. 4c shows the difference in 850-hPa temperature anomaly between C19Q and PRE. The areas of 850-hPa anomaly increases (decreases) correspond well to the locations where GHCN stations also reported increases (decreases) in surface air temperature anomaly for the same periods. Further, the AIRS warming zone in Fig. 2c coincides with a region of 850-hPa warm anomalies, which represents a much more direct explanation for the warming than the AOD reduction in Fig. 2d.

To the first order, synoptic atmospheric mechanisms were positioned to facilitate the surface temperature evolution from PRE to C19Q. While the AOD decreases in Fig. 2d qualitatively correspond to the AIRS warming in Fig. 2c, synoptic atmospheric patterns inferred from 850-hPa temperature more closely match the both pattern and magnitude of the temperature evolution in Fig. 2 and Fig. 4c. Though 850-hPa temperature provides a broad-scale synoptic explanation for the C19Q temperatures, aerosol direct effect warming may have nonetheless been super-imposed upon the 850-hPa pattern.

3.2. VIIRS aerosol analysis

The optical properties shown in Fig. 2d do not necessarily indicate a reduction in anthropogenic particulate concentrations. To more directly assess changes in anthropogenic aerosols versus natural sources of aerosols, such as mineral dust and biomass burning, the VIIRS Level 2

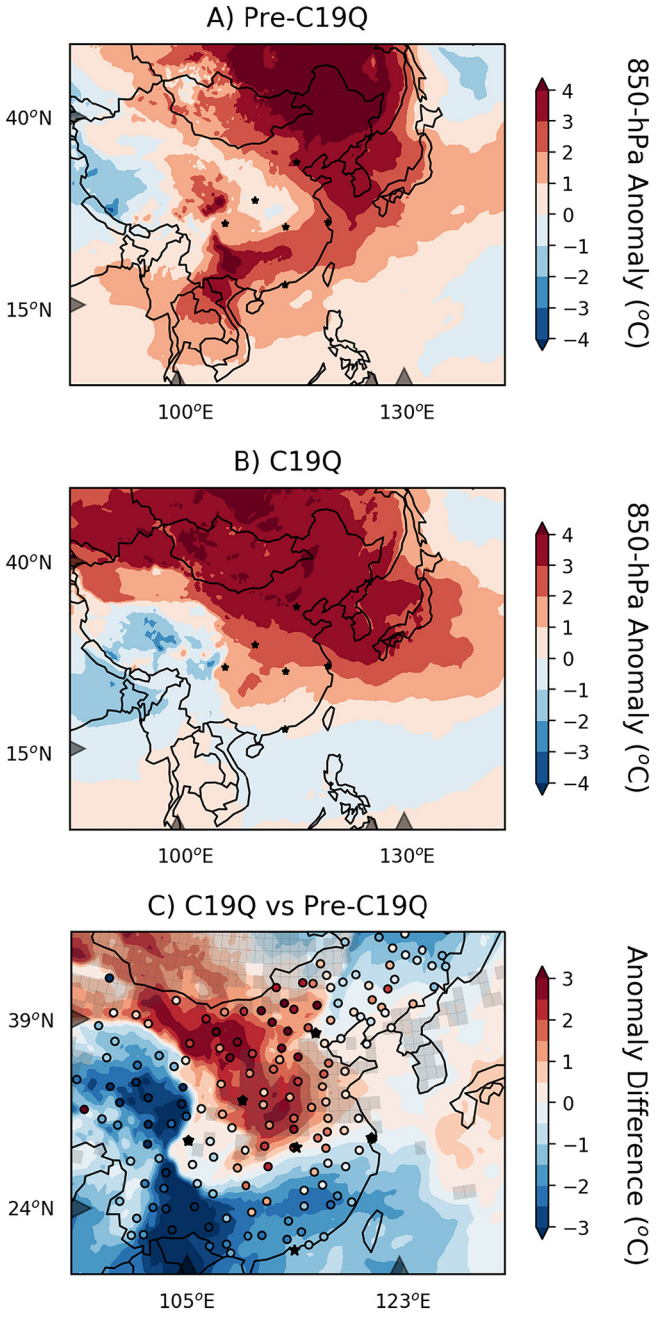

Fig. 4. ERA5 850-hPa temperature anomaly for the PRE (A) and C19Q (B) periods computed against the 1979–2020 mean. The difference between 850-hPa anomalies (i.e., C19Q – PRE) is shown in (C) along with the GHCN station markers from Fig. 3 which are plotted using the same color scale from that image. The *Aqua* AIRS pixels that detected increases in the daily mean temperature anomaly between C19Q and PRE from Fig. 2c are also shown as semi-transparent gray cells. Note that the 850-hPa surface is below ground for some high-elevation terrain, and ERA5 is visualizing extrapolated temperatures at these locations.

aerosol type diagnosis is assessed. Because the VIIRS AOD processing algorithm identifies urban aerosols as largely fine-mode particulates (i.e., $PM_{2.5}$) (Laszlo and Liu, 2016), the change in urban aerosol fraction between the C19Q and PRE periods reflects changes both in primary emission and as well as secondary formation.

Fig. 5 shows the percent change in urban aerosol fraction using the method described in Section 2.1. Overall, the locations shown in Fig. 5 experienced a decline from 27.1% PRE urban aerosols to 17.5% urban aerosols composition during C19Q, a reduction of −34.1%. While urban aerosol fraction declined across most of east China, areas near Shanghai and Beijing experienced a +62.3% and +65.9% increase, respectively. In fact, urban aerosol fraction increased during C19Q across nearly the entire Bohai Economic Rim, which encompasses the Tianjin-Beijing megacity. Meanwhile, urban aerosol fraction declined −38.2% in the greater Wuhan area. As will be discussed in Section 4, these patterns closely align with other COVID-19 air quality analyses.

3.3. Modeling analysis

The urban aerosol changes in Fig. 5a are used to force the WRF-Chem experiment. In the BASE simulation, all emissions are represented using the RETRO/EDGAR dataset, whereas in the REDUX simulation, the emissions of both particulate species (PM_{10} and $PM_{2.5}$) are proportional to the urban aerosol reductions (or increases) as shown in Fig. 5b. The REDUX T_{AVG} correlates strongly with observed T_{AVG} at 153 GHCN sites within the WRF-Chem domain. Collectively, the REDUX T_{AVG} explains 92% of the observed T_{AVG} variability during the C19Q period (Fig. 6a). Further, WRF-Chem capably reproduces the shape of the T_{AVG} time series as the example from Wuhan illustrates (Fig. 7).

Though WRF-Chem mirrors the Wuhan 2-m temperature time series in Fig. 7, a −1.75 °C cold bias is evident. Fig. 6b expands the REDUX bias spatially to show that 1–3 °C cool biases are common across southeast China with cool biases increasing to ~5 °C in the northern and western areas of the domain. The domain-wide cold bias is −4.3 °C for all 153 stations. As Fig. 6b indicates, WRF-Chem struggled in the higher elevation portions of interior China but performed more accurately in the lower elevations. If stations >500 m are excluded, then REDUX explains 99% of the GHCN T_{AVG} variability (Fig. 6c). Fig. 6d shows the 83 stations located below 500-m elevation which possess a − 3.3 °C bias. Regardless, the WRF-Chem simulations accurately capture the timing and persistence of air mass changes (Fig. 7), such that they can confidently be compared to determine the magnitude of any aerosol direct effect warming.

Fig. 8a shows the T_{AVG} difference between the REDUX and BASE simulations, communicating the warming/cooling resulting from the change in anthropogenic particulate emissions forced upon the model. The largest area of increased T_{AVG} is concentrated south of Chengdu and Wuhan where temperatures warmed between +0.2–0.3 °C. In Wuhan specifically, C19Q warming was 0.19 °C with the largest modeled warming at any GHCN site occurring at Siping in the northwest corner of Fig. 8a. The modeled warming captures the footprint of GHCN anomaly changes reasonably well. Even the maximum REDUX warming in Siping (+0.29 °C) corresponds to a corridor of GHCN-detected T_{AVG} increase. Though the GHCN T_{AVG} changes (Figs. 3, 8a) are roughly an order of magnitude greater than the WRF-Chem warming (Fig. 8a), areas that witnessed increases in in-situ temperature anomalies generally experienced increases in REDUX T_{AVG} as well. The reverse is also true with WRF-Chem producing either cooling or near-zero T_{AVG} change along the eastern and southern coastlines, as well as pronounced cooling along the western edge of the Fig. 8a. The order-of-magnitude discrepancy between REDUX and GHCN temperature changes during the lockdown emphasizes that synoptic atmospheric patterns (Fig. 4c) were the driving warming mechanism, but the close spatial agreement suggests altered emissions may have also played a contributing role.

To statistically interrogate this relationship, Fig. 8b shows a scatterplot between the WRF-Chem modeled warming and the GHCN observed T_{AVG} anomaly changes. An F test confirms a statistically significant (F Ratio = 15.8; $p < 0.01$) positive correlation, and also shows that the REDUX warming explains 8.5% of the variability in GHCN T_{AVG} warming during the C19Q period. The small p-value associated with the regression relationship rejects the null hypothesis that the in-situ temperature evolution is unrelated to the aerosol direct effect warming. As described above, Fig. 8c confirms that the 850-hPa temperature evolution is a much stronger source of GHCN anomaly patterns than REDUX

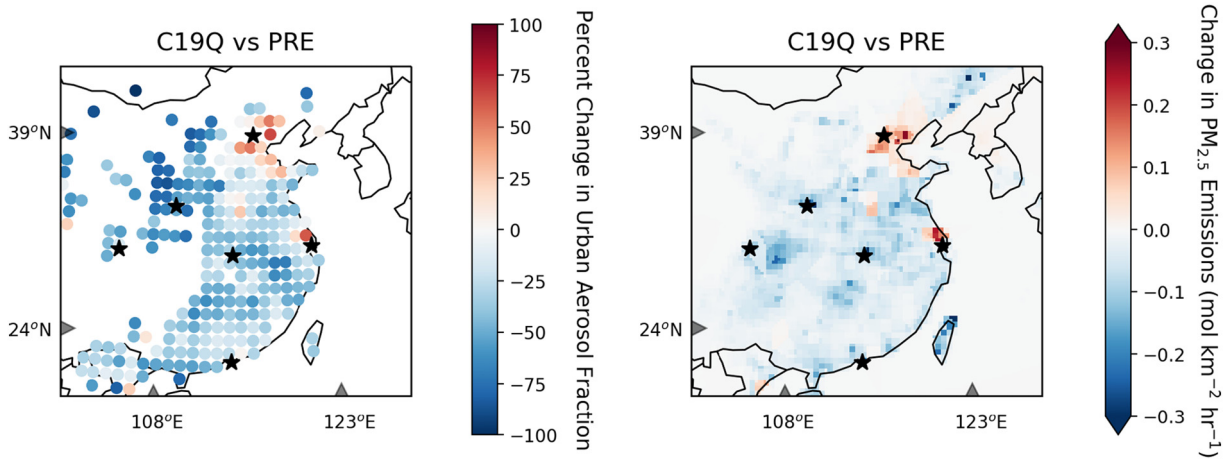

Fig. 5. Percent change in the urban aerosol fraction detected by the *NOAA-20* VIIRS instrument between the PRE and C19Q periods (left). For instance, a decrease in urban aerosol fraction from 0.30 during PRE to 0.15 during C19Q would yield and −50% change. The change in VIIRS-based urban aerosols was then passed into the WRF-Chem emissions input files. The absolute change in $PM_{2.5}$ anthropogenic emissions, based on the percent increase/decrease detected by VIIRS, that was forced upon the REDUX simulation is shown (right).

warming, explaining 58.3% of the variability (F Ratio = 237.8; $p < 0.01$). However, when the REDUX warming and 850-hPa anomaly changes are combined into a single multivariate statistical model (Eq. 1), the predictions for the GHCN anomaly changes improve. The R^2 for Eq. 1 is 0.622, with both variables contributing significantly to the predictive expression, versus 0.583 for 850-hPa temperature only (Fig. 8c).

$$GHCN_{C19Q\ \Delta T} = 0.13 + 6.06{*}WRF_{REDUX-BASE} + 0.82{*}850{-}hPa_{C19Q\ \Delta T} \quad (1)$$

Thus, the addition of aerosol direct effect warming improves the representation of surface temperature warming beyond what could be gleaned from 850-hPa temperature alone.

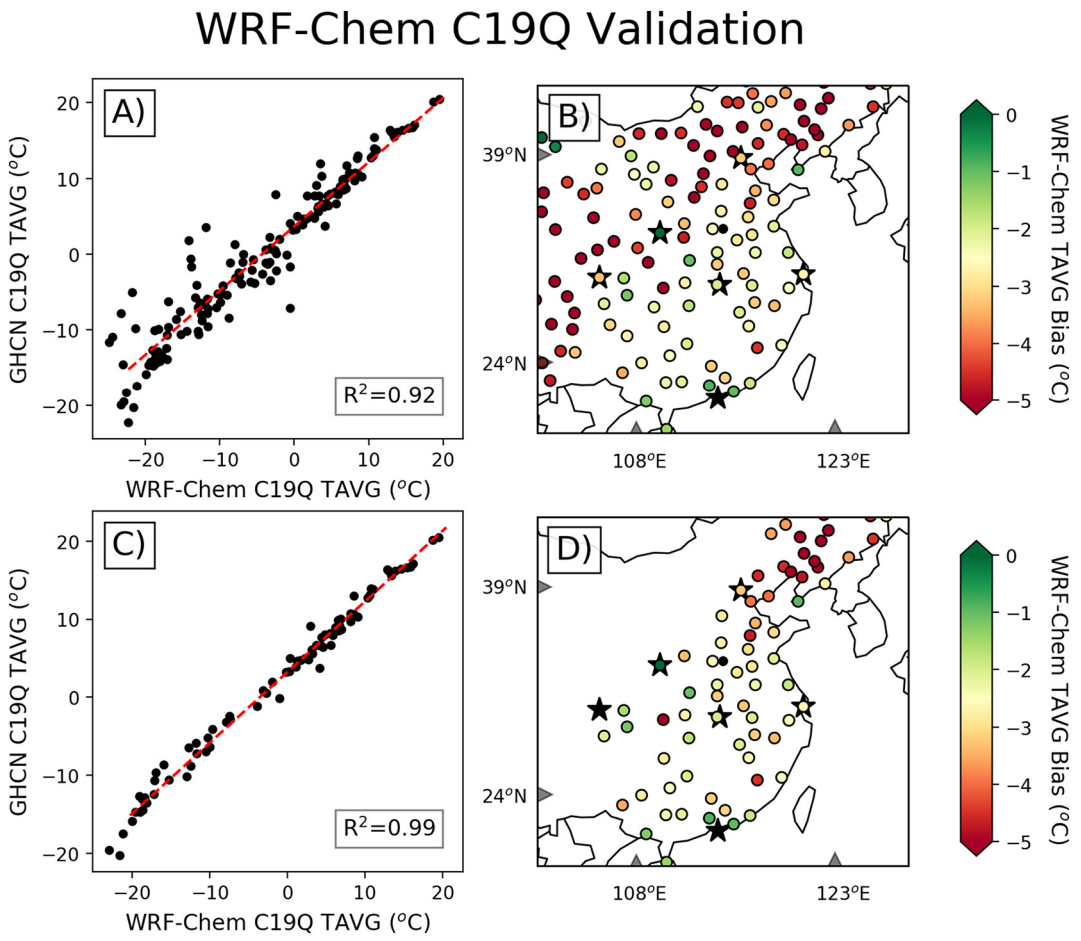

Fig. 6. REDUX T_{AVG} versus the 153 GHCN T_{AVG} for the C19Q period (A), as well as the mean REDUX T_{AVG} bias for the same period compared to the GHCN (B). Panes (C) and (D) reproduce (A) and (B), respectively; however, only stations beneath 500-m elevation are shown. The dashed red line in (A) and (C) is the least squares regression relationship, which is significant in both cases with >99% confidence (i.e., $p < 0.01$). The coefficient of determination (R^2) is shown for both relationships.

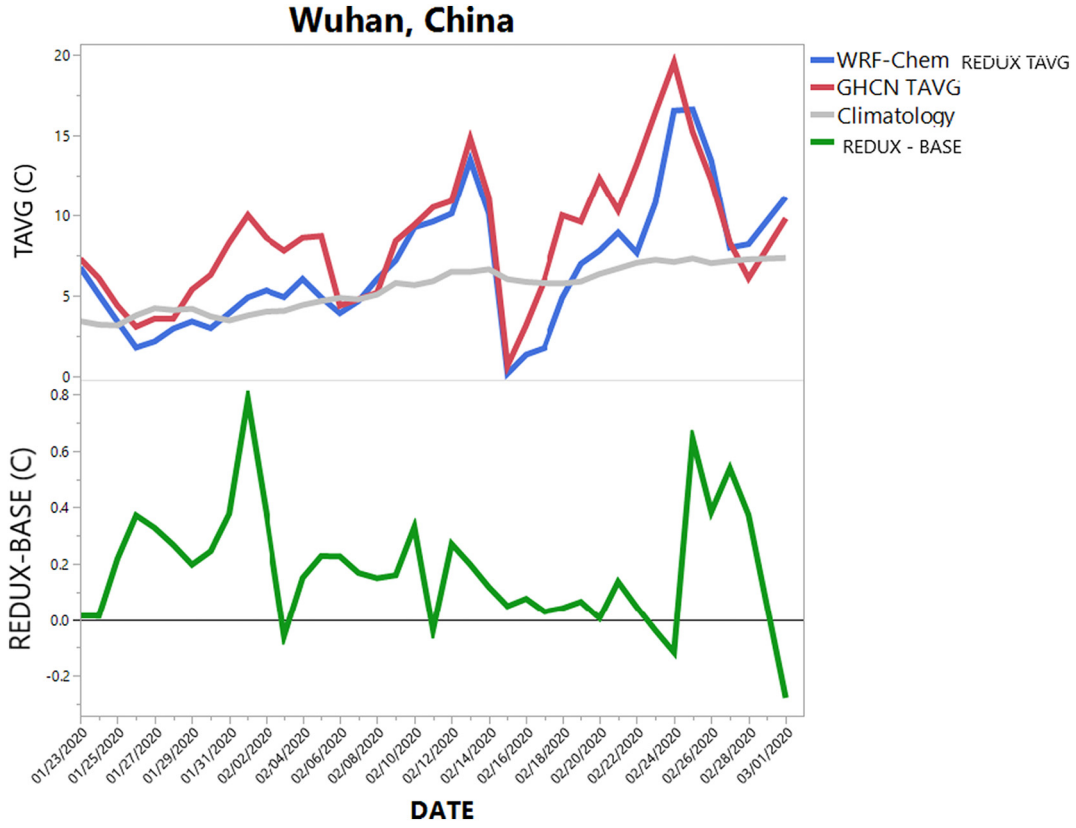

Fig. 7. Time series of the REDUX T_{AVG} (blue) and GHCN T_{AVG} (red) for the C19Q period (top) for Wuhan, China. The climatological daily TAVG for the Wuhan GHCN is shown gray. The difference between REDUX and BASE (i.e., the temperature change that occurred when particulate emissions were modified) is shown in the bottom pane.

4. Discussion

4.1. Physical findings

The results described in Section 3 support recent work pertaining to the COVID-19 pandemic as well as the existing body of research related to east Asian air quality. Though Diamond and Wood (2020) note that industrial and power generation activities, which account for >90% of particulate emissions, were less effected by the lockdown (~20% reduction), our VIIRS-based analysis in Section 3.2 nonetheless detected a 34.1% decrease in urban aerosol fraction. This value soundly agrees with other recent observations, affirming our method to force the WRF-Chem REDUX simulation. For comparison, a study of in-situ PM measurements in Wuhan found decreases of 41.2% and 33.1% for $PM_{2.5}$ and PM_{10}, respectively (Sulaymon et al., 2021), with another identifying a 36.9% decline in $PM_{2.5}$ (Lian et al., 2020). Meanwhile, several studies have highlighted the persistence of haze events despite the emissions decline in Beijing-Tianjin (e.g., Le et al., 2020; Su et al., 2020; Wang et al., 2020a; Zhao et al., 2020) and Shanghai (Chang et al., 2020). VIIRS confirms the increase in urban aerosol fraction in these areas, which Kroll et al. (2020) thoroughly explain as being a complex function of meteorology and chemistry rather than a simple product of emission. Specifically, Su et al. (2020) determined an average decrease in $PM_{2.5}$ of 19% over northern China, compared to the VIIRS-based increase of 25% average over a comparable area.

The WRF-Chem modeling experiment also study found that the changes in urban aerosol fraction were associated with sub-degree warming over parts of China. As mentioned in Section 1, other investigations of aerosol radiative effects have concluded temperature changes over east China ranging from +0.13 °C (Gettelman et al., 2020), +0.05–0.15 °C (Yang et al., 2020), and +0.30 °C (Diffenbaugh et al., 2020). Our analysis strongly resonates with these studies, with +0.19 °C warming in Wuhan proper and > 0.2 °C increases to the south and southwest (Fig. 8a). Although a single experiment (rather than an ensemble of multiple experiments with different parameterizations) was performed, the strong alignment of our work with previous findings suggest the physics schemes in Table 1 and the implementation of VIIRS-based emission changes appropriately captured the modified radiative forcing. The broad, >0.2 °C warming zone south and southwest of Wuhan is puzzling given that it is displaced from the area VIIRS detected the largest reduction in urban aerosol fraction (Fig. 5a). Additionally, the displacement cannot be driven by secondary PM formation because such interactions were intentionally not parameterized in the GOCART aerosol scheme. Future research may engage this displacement in more detail by drawing upon Lagrangian back-trajectory models, such as HYSPLIT.

While the warm February 2020 conditions in east China were noted by Diamond and Wood (2020), this is the first attempt to connect the pattern of temperature anomalies to the change in anthropogenic activity. Though the magnitude of PRE versus C19Q GHCN anomalies was largely explained by 850-hPa temperature patterns, WRF-Chem resolved aerosol direct effect warming that generally matched the areas with observed GHCN anomalies (Fig. 8a). Though the REDUX warming was roughly an order of magnitude smaller than the GHCN anomaly changes, the time series from Wuhan (Fig. 7) shows that it exceeded 0.5 °C on three separate days (1, 25, and 27 February 2020), with a maximum of +0.78 °C on 1 February 2020. When intra-daily variation is considered, the maximum warming was +1.76 °C at 0000 UTC 13 February 2020. These values are consistent with short-duration, event-specific studies of aerosol- and haze-related cooling in east China (i.e., increased PM reduces incoming radiation rather than reduced PM enhancing incoming radiation). During a severe January 2013 haze event, aerosol radiative effects were found to cool surface temperatures by ~1 °C in Hubei province, including Wuhan, with decreases in the

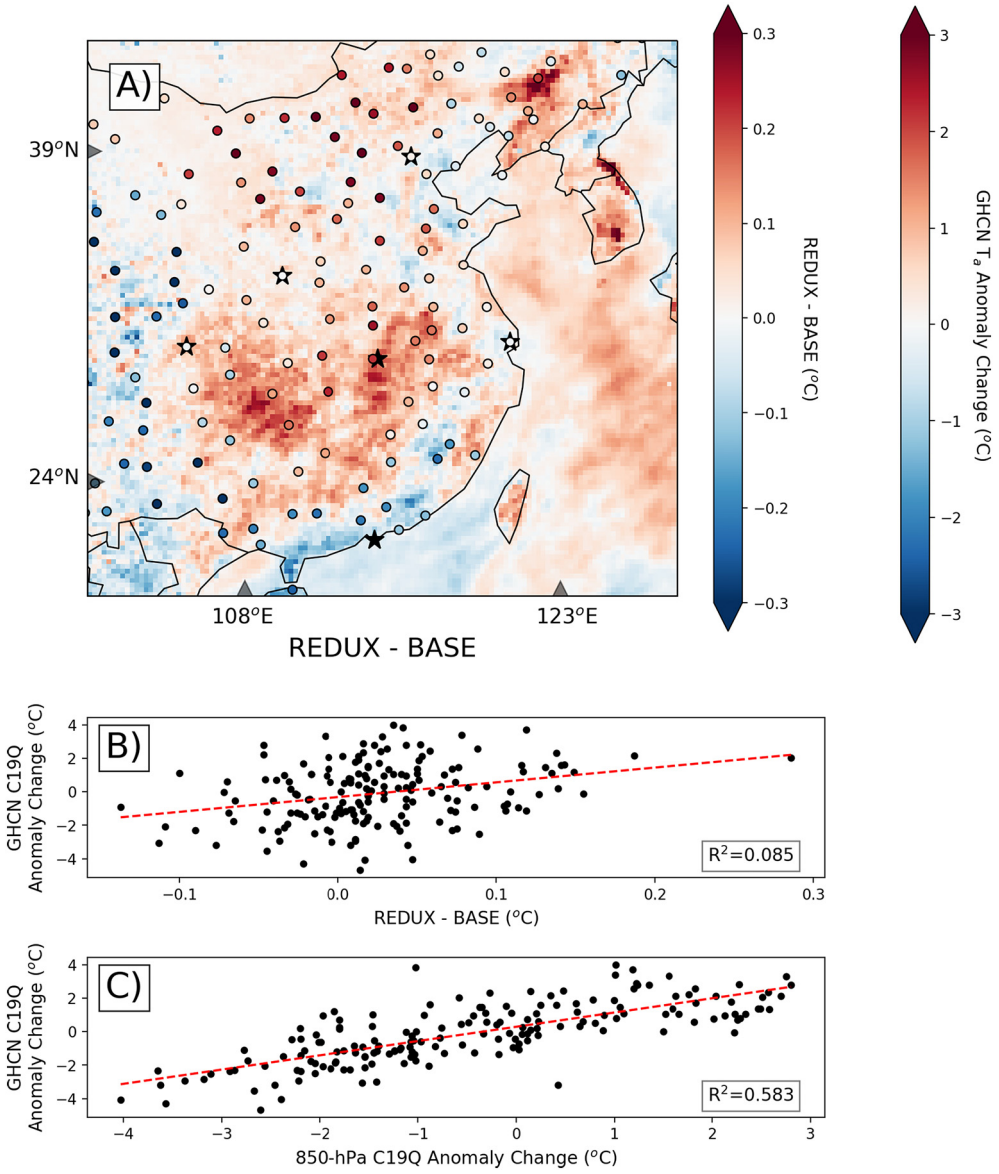

Fig. 8. The difference between REDUX and BASE (i.e., the temperature change that occurred when particulate emissions were modified) plotted alongside the observed change in GHCN T_{AVG} anomaly shown in Fig. 3 (A). This map essentially compares how much surface temperatures actually changed during C19Q versus the temperature change generated by the VIIRS-modified WRF-Chem simulation. For each GHCN station, the observed T_{AVG} anomaly change is plotted against the REDUX temperature change (B) and the 850-hPa anomaly change from Fig. 4c (C). The dashed red line in (B) and (C) is the regression relationship, which is significant in both cases with >99% confidence (i.e., $p < 0.01$). The coefficient of determination (R^2) is shown for both relationships.

Sichuan Basin exceeding 2 °C (Zhang et al., 2015a). Similarly, modeling results from a haze episode in the north China plain identified aerosol radiative cooling approaching 3 °C in some locations. A separate study conducted over the Beijing megacity during August 2008 identified smaller aerosol direct effect cooling at the surface that varied between 0.90 °C and 0.45 °C (Jin et al., 2010).

This study also incorporates an important methodological distinction from the aforementioned severe haze research that would predispose it to identify smaller temperature changes. Because nearly all COVID-19 meteorology/climate studies have permitted emissions during the lockdown, though at a reduced level, they deviate from the existing body of aerosol-related temperature changes. Such studies typically compare "polluted" and "control" simulations which correspond to one chemistry-enabled simulation and another simulation in which aerosol radiative feedbacks are entirely suppressed (e.g., M. Gao et al., 2016; Zhang et al., 2015a). Thus, this study and others improve upon prior meteorological air quality modeling by still allowing emissions in the cleaner scenario but reducing them as guided by contemporaneous observations. Logically, any thermodynamic responses would be more muted in this case because emissions were still represented at a significant fraction of their baseline value. Additionally, whereas other COVID-19 studies reduce emissions on a national scale using country-wide (e.g., Gettelman et al., 2020) or province-wide (Yang et al., 2020) emission inventories, Section 2 describes how the particulate emissions are spatially varied based on the results of an urban aerosol analysis with the *NOAA-20* VIIRS instrument.

4.2. Implications for public health

Although the REDUX temperature increases and similar warming found by other studies (Diffenbaugh et al., 2020; Gettelman et al., 2020; Yang et al., 2020) are small in magnitude, the implications for public health weigh larger. The discussion below includes simple calculations drawing upon recent COVID-19 transmission-temperature studies, but it only does so to communicate the relevance of a lockdown-warming-transmission feedback, which transcends the

current pandemic. This section is intended to synthesize recent lockdown-warming findings with a larger body of disease transmission research, which have not been synthesized to date.

Historically, temperature has been tied to the transmission of communicable diseases, particularly the Severe Acute Respiratory Syndrome (SARS) (Chan et al., 2011; K. U. N. Lin et al., 2006) and the seasonal influenza (Shaman and Karspeck, 2012; Shaman et al., 2010; Tamerius et al., 2011). As the COVID-19 pandemic has rapidly spread across the globe, infectious disease experts have explored the relationship between meteorological conditions and the transmissibility of SARS-CoV-2, the virus responsible for the COVID-19 illness. Though research into the relationship between temperature and COVID-19 transmissibility is still ongoing, results are mixed. Whereas some studies have identified negative relationships between air temperature, humidity, and/or ultraviolet radiation and COVID-19 infections (e.g., Lolli et al., 2020; Ma et al., 2020; Prata et al., 2020; Tobías and Molina, 2020; Tosepu et al., 2020; Xu et al., 2020), others have concluded that no such relationship exists (e.g., Briz-Redón and Serrano-Aroca, 2020; Sajadi et al., 2020; Yao et al., 2020). Further, findings vary according to the shape of the temperature-transmission relationship (e.g., linear, quadratic), the metric used to express transmission (e.g., relative risk, new infections), lag effects (e.g., 0, 1, 2 days), and the temperature range over which it applies (i.e., warmer temperatures diminish transmission up to a threshold). Regardless, SARS-CoV-2 transmission modeling incorporating temperature effects has quickly emerged with careful projections already accruing thousands of citations (Kissler et al., 2020).

As a public health example, the REDUX temperature changes from Section 3.3 are paired with recent COVID-19 transmission metrics to illustrate the effect of tenths-of-degree lockdown-driven warming on the spread of a temperature-dependent pathogen (which may ultimately exclude SARS-CoV-2). For our illustration, we apply the result of Wang et al. (2020b) to February 2020 infection dynamics in Wuhan. Wang et al. (2020b) identified a 0.026 reduction in the COVID-19 effective reproductive number (R_{eff}) for every 1 °C increase in temperature. In the field of infectious disease, R_{eff} represents the number of secondary infections generated by one infected person in light of population immunity, and for COVID-19, social distancing measures (Anderson et al., 2020). Extending the meteorological findings determined here, the REDUX warming would have decreased R_{eff} by 0.0049 in Wuhan, leading to a decrease of 1411 cases during February 2020 (SI Eq. 1). In the longest serial interval (the elapsed time between successive cases in the same transmission chain) (19 days) and lowest R_{eff} (1.4) scenario (Li et al., 2020), infections are only reduced by 64. However, the shortest serial interval (5.3 days) and highest R_{eff} (3.9) scenario (Wang et al., 2020b), then the REDUX warming reduces February infections in Wuhan by 106,458. See the Supplementary Information for more detail.

Many estimates of R_{eff} have been developed for COVID-19 (Liu et al., 2020a), and they will likely continue to change as more data becomes available, particularly as the transmissibility of different strains and data from the 2020–2021 boreal winter surge are digested. The purpose of the computations above is not to produce an actual estimate of individuals whose infections were prevented by aerosol radiative effects, but to illustrate the cumulative effect of even a tenths-of-degree temperature change when multiplied over a weeks-long period in a highly populated area. In fact, the specific R_{eff} and serial interval are almost irrelevant considering public health lockdowns can be implemented for any number of future infectious diseases with unique transmission dynamics. For instance, a recent study compared COVID-19 transmission to other *Betacoronaviruses* (the genus containing SAR-CoV-2), which includes SARS-CoV-1, the Middle East respiratory syndrome (MERS) coronavirus, HCoV-OC43, and HCoV-HKU1. Winter versus summer R_0 values (similar to R, but assumes the population is entirely susceptible) declined from 2.2 to 1.7 for both for HCoV-OC43 and HCoV-HKU1, indicating the reduction in coronavirus transmission during warmer summer months (Kissler et al., 2020). Similarly, in New York state, R_0 for the influenza virus declines by roughly 40% from 2.5 to 1.5 between January and July (Shaman et al., 2010). While the tenths-of-degree REDUX temperature increases are two orders of magnitude lower than the tens-of-degrees winter-to-summer seasonal temperature swing, these findings nonetheless suggest that quarantine-related warming may, in some marginal fashion, retard temperature-dependent disease transmission during mandated lockdowns. Additionally, a future disease outbreak resulting in a similar lockdown and air pollution reduction could prompt a more pronounced temperature response depending on the specific synoptic pattern and season.

5. Conclusions

Disease mitigation strategies, such as restricted population movement, can improve air quality by reducing anthropogenic pollution emissions. However, clean air allows more incoming solar radiation to reach earth's surface than polluted air, such that the atmosphere's radiation budget may be non-trivially altered by abrupt, dramatic reductions in anthropogenic emissions. The analyses in Section 3 reveal that the surface temperatures in east China during the COVID-19 quarantine period were largely explained by synoptic patterns, as characterized by 850-hPa air temperature. Numerical weather simulations forced by a satellite analysis of urban aerosol reductions revealed that aerosol-driven warming was an order of magnitude smaller than what was measured by the surface stations. Nonetheless, in regards to the first question posed in Section 1, statistical testing revealed that the simulated aerosol radiative effect warming was a small, yet significant, contribution to the temperature patterns observed during China's COVID-19 quarantines.

Recent studies have determined that COVID-19-related aerosol reductions prompted sub-degree warming over east China, ranging from +0.13 °C (Gettelman et al., 2020), +0.05–0.15 °C (Yang et al., 2020), and +0.30 °C (Diffenbaugh et al., 2020). This present work confirms previous research, identifying +0.19 °C in Wuhan and supporting the idea of quarantine-related warming. Because the spread of some communicable diseases varies with temperature, the presence of a lockdown-warming-transmission feedback has implications for public health well beyond COVID-19. Regarding the second research question in Section 1, simple epidemiological calculations (SI Eq. 1) show that even tenths-of-degree warming over an outbreak zone can non-trivially influence cases of infection.

Though preliminary (and hotly debated) transmission metrics for COVID-19 are used to illustrate the public health ramifications of the tenths-of-degree warming, the conceptual implications of altered transmissions dynamics due to marginal warming extend to any temperature-dependent communicable disease. These findings are relevant for public health officials as they consider the consequences of infectious disease containment. The aerosol-driven warming documented by this study may serve as an additional motivation for instituting mobility restrictions in large, pollution-prone urban areas. However, because some studies have suggested that SARS-CoV-2 transmission is most efficient within a range of temperatures (Haque and Rahman, 2020; Huang et al., 2020b), lockdown-driven warming may be counter-productive if it shifts a region into a more efficient transmission range. Consequently, public health officials should closely monitor the emergence of new epidemiological studies of SARS-CoV-2 temperature-transmission dynamics as they weigh the findings of this work. Future holistic analyses of the effectiveness of quarantines need to account for reduced mobility, improved air quality, and meteorological feedbacks in order fully understand their effects on disease transmission.

CRediT authorship contribution statement

P.W. Miller: Conceptualization, Formal analysis, Writing – original draft, Project administration. **C. Reesman:** Investigation, Data curation. **M.K. Grossman:** Writing – review & editing. **S.A. Nelson:** Investigation. **V. Liu:** Software. **P. Wang:** Writing – review & editing.

Declaration of competing interest

The authors declare that they have no known competing financial interests or personal relationships that could have appeared to influence the work reported in this paper.

Acknowledgments

This work was funded by the National Science Foundation's Physical and Dynamic Meteorology program (AGS 2027199), and the computational resources for this work were provided by the Louisiana State University Center for Computation Technology. The authors thank the anonymous reviewers for their comments improving the manuscript and Erica Lehnert for assistance facilitating author interactions. All satellite and in-situ data analyzed in this study is either already available in freely accessible web archive maintained by NASA (https://giovanni.gsfc.nasa.gov/giovanni/) or the National Centers of Environmental Information (https://gis.ncdc.noaa.gov/maps/ncei/cdo/daily). *NOAA-20* VIIRS Level 2 data was provided by Shobha Kondragunta from NESDIS Center for Satellite Applications and Research. The WRF-Chem BASE and REDUX T_{AVG} files will be made publicly available on Zenodo (https://zenodo.org/) as well as https://faculty.lsu.edu/paulmiller/research_data.php.

Appendix A. Supplementary data

Supplementary data to this article can be found online at https://doi.org/10.1016/j.scitotenv.2021.146579.

References

Anderson, R.M., Heesterbeek, H., Klinkenberg, D., Hollingsworth, T.D., 2020. How will country-based mitigation measures influence the course of the COVID-19 epidemic? Lancet 395 (10228), 931–934. https://doi.org/10.1016/S0140-6736(20)30567-5.

Aumann, H.H., Chahine, M.T., Gautier, C., Goldberg, M.D., Kalnay, E., McMillin, L.M., ... Susskind, J., 2003. AIRS/AMSU/HSB on the aqua mission: design, science objectives, data products, and processing systems. IEEE Trans. Geosci. Remote Sens. 41 (2), 253–264. https://doi.org/10.1109/TGRS.2002.808356.

Briz-Redón, Á., Serrano-Aroca, Á., 2020. A spatio-temporal analysis for exploring the effect of temperature on COVID-19 early evolution in Spain. Sci. Total Environ. 728, 138811. https://doi.org/10.1016/j.scitotenv.2020.138811.

Bujin, B., Joshua S.A., Dylan BM., Allen, R., Kelley C.W., & Julian D.M. (2020). PM2.5 and ozone air pollution levels have not dropped consistently across the us following societal Covid response.

Chan, K.H., Peiris, J.S.M., Lam, S.Y., Poon, L.L.M., Yuen, K.Y., Seto, W.H., 2011. The effects of temperature and relative humidity on the viability of the SARS coronavirus. Advance Virol. 2011, 734690. https://doi.org/10.1155/2011/734690.

Chang, Y., Huang, R.-J., Ge, X., Huang, X., Hu, J., Duan, Y., ... Lehmann, M.F., 2020. Puzzling haze events in China during the coronavirus (COVID-19) shutdown. Geophys. Res. Lett. 47 (12). https://doi.org/10.1029/2020GL088533 e2020GL088533.

Crippa, M., Guizzardi, D., Muntean, M., Schaaf, E., Dentener, F., van Aardenne, J.A., ... Janssens-Maenhout, G., 2018. Gridded emissions of air pollutants for the period 1970–2012 within EDGAR v4.3.2. *Earth Syst. Sci.* Data 10 (4), 1987–2013. https://doi.org/10.5194/essd-10-1987-2018.

Diamond, M.S., Wood, R., 2020. Limited regional aerosol and cloud microphysical changes despite unprecedented decline in nitrogen oxide pollution during the February 2020 COVID-19 shutdown in China. Geophys. Res. Lett. 47 (17). https://doi.org/10.1029/2020GL088913 e2020GL088913.

Diffenbaugh, N.S., Field, C.B., Appel, E.A., Azevedo, I.L., Baldocchi, D.D., Burke, M., ... Wong-Parodi, G., 2020. The COVID-19 lockdowns: a window into the earth system. Nat. Rev. Earth Environ. https://doi.org/10.1038/s43017-020-0079-1.

Donzelli, G., Cioni, L., Cancellieri, M., Llopis Morales, A., Morales Suárez-Varela, M.M., 2020. The effect of the Covid-19 lockdown on air quality in three Italian medium-sized cities. Atmosphere 11 (10). https://doi.org/10.3390/atmos11101118.

Forster, P.M., Forster, H.I., Evans, M.J., Gidden, M.J., Jones, C.D., Keller, C.A., ... Turnock, S.T., 2020. Current and future global climate impacts resulting from COVID-19. Nat. Clim. Chang. 10 (10), 913–919. https://doi.org/10.1038/s41558-020-0883-0.

Fu, F., Purvis-Roberts, K.L., Williams, B., 2020. Impact of the COVID-19 pandemic lockdown on air pollution in 20 major cities around the world. Atmosphere 11 (11). https://doi.org/10.3390/atmos11111189.

Gao, Y., Zhao, C., Liu, X., Zhang, M., Leung, L.R., 2014. WRF-Chem simulations of aerosols and anthropogenic aerosol radiative forcing in East Asia. Atmos. Environ. 92, 250–266. https://doi.org/10.1016/j.atmosenv.2014.04.038.

Gao, M., Carmichael, G.R., Wang, Y., Saide, P.E., Yu, M., Xin, J., ... Wang, Z., 2016. Modeling study of the 2010 regional haze event in the North China plain. Atmos. Chem. Phys. 16 (3), 1673–1691. https://doi.org/10.5194/acp-16-1673-2016.

Gettelman, A., Lamboll, R., Bardeen, C.G., Forster, P.M., Watson-Parris, D., 2020. Climate impacts of COVID-19 induced emission changes. Geophys. Res. Lett. https://doi.org/10.1029/2020GL091805 n/a(n/a), e2020GL091805.

Ginoux, P., Chin, M., Tegen, I., Prospero, J.M., Holben, B., Dubovik, O., Lin, S.-J., 2001. Sources and distributions of dust aerosols simulated with the GOCART model. J. Geophys. Res.-Atmos. 106 (D17), 20255–20273. https://doi.org/10.1029/2000JD000053.

Grell, G.A., Peckham, S.E., Schmitz, R., McKeen, S.A., Frost, G., Skamarock, W.C., Eder, B., 2005. Fully coupled "online" chemistry within the WRF model. Atmos. Environ. 39 (37), 6957–6975. https://doi.org/10.1016/j.atmosenv.2005.04.027.

Haque, S.E., Rahman, M., 2020. Association between temperature, humidity, and COVID-19 outbreaks in Bangladesh. Environ. Sci. Pol. 114, 253–255. https://doi.org/10.1016/j.envsci.2020.08.012.

Hersbach, H., Bell, B., Berrisford, P., Hirahara, S., Horányi, A., Muñoz-Sabater, J., ... Thépaut, J.-N., 2020. The ERA5 global reanalysis. Q. J. R. Meteorol. Soc. https://doi.org/10.1002/qj.3803 n/a(n/a).

Huang, R.-J., Zhang, Y., Bozzetti, C., Ho, K.-F., Cao, J.-J., Han, Y., ... Prévôt, A.S.H., 2014. High secondary aerosol contribution to particulate pollution during haze events in China. Nature 514 (7521), 218–222. https://doi.org/10.1038/nature13774.

Huang, X., Ding, A., Gao, J., Zheng, B., Zhou, D., Qi, X., ... He, K., 2020a. Enhanced secondary pollution offset reduction of primary emissions during COVID-19 lockdown in China. Natl. Sci. Rev. https://doi.org/10.1093/nsr/nwaa137.

Huang, Z., Huang, J., Gu, Q., Du, P., Liang, H., Dong, Q., 2020b. Optimal temperature zone for the dispersal of COVID-19. Sci. Total Environ. 736, 139487. https://doi.org/10.1016/j.scitotenv.2020.139487.

Huang, J., Zhang, L., Liu, X., Wei, Y., Liu, C., Lian, X., ... Zhang, T., 2020c. Global prediction system for COVID-19 pandemic. Sci. Bull. 65 (22), 1884–1887. https://doi.org/10.1016/j.scib.2020.08.002.

IPCC, 2014. Climate change 2014: synthesis report. Contribution of working groups I, II and III to the fifth assessment report of the intergovernmental panel on climate change. In: Pachauri, R.K., Meyer, L.A. (Eds.), Core Writing Team. IPCC, Geneva, Switzerland pp. 151 pp.

Jamil, T., Alam, I., Gojobori, T., Duarte, C.M., 2020. No evidence for temperature-dependence of the COVID-19 epidemic. Front. Public Health 8, 436.

Jia, C., Fu, X., Bartelli, D., Smith, L., 2020. Insignificant impact of the "stay-at-home" order on ambient air quality in the Memphis metropolitan area, USA. Atmosphere 11 (6), 630.

Jin, M., Shepherd, J.M., Zheng, W., 2010. Urban surface temperature reduction via the urban aerosol direct effect: a remote sensing and WRF model sensitivity study. Adv. Meteorol. 2010. https://doi.org/10.1155/2010/681587.

Kissler, S.M., Tedijanto, C., Goldstein, E., Grad, Y.H., Lipsitch, M., 2020. Projecting the transmission dynamics of SARS-CoV-2 through the postpandemic period. Science 368 (6493), 860. https://doi.org/10.1126/science.abb5793.

Kroll, J.H., Heald, C.L., Cappa, C.D., Farmer, D.K., Fry, J.L., Murphy, J.G., Steiner, A.L., 2020. The complex chemical effects of COVID-19 shutdowns on air quality. Nat. Chem. 12 (9), 777–779. https://doi.org/10.1038/s41557-020-0535-z.

Laszlo, I., Liu, H., 2016. EPS aerosol optical depth (AOD) algorithm theoretical basis document. NOAA NESDIS Center for Satellite Applications and Research Retrieved from. https://www.star.nesdis.noaa.gov/jpss/documents/ATBD/ATBD_EPS_Aerosol_AOD_v3.0.1.pdf.

Le, T., Wang, Y., Liu, L., Yang, J., Yung, Y.L., Li, G., Seinfeld, J.H., 2020. Unexpected air pollution with marked emission reductions during the COVID-19 outbreak in China. Science 369 (6504), 702. https://doi.org/10.1126/science.abb7431.

Li, Q., Guan, X., Wu, P., Wang, X., Zhou, L., Tong, Y., ... Feng, Z., 2020. Early transmission dynamics in Wuhan, China, of novel coronavirus–infected pneumonia. N. Engl. J. Med. 382 (13), 1199–1207. https://doi.org/10.1056/NEJMoa2001316.

Lian, X., Huang, J., Huang, R., Liu, C., Wang, L., Zhang, T., 2020. Impact of city lockdown on the air quality of COVID-19-hit of Wuhan city. Sci. Total Environ. 742, 140556. https://doi.org/10.1016/j.scitotenv.2020.140556.

Lin, J.T., McElroy, M.B., 2011. Detection from space of a reduction in anthropogenic emissions of nitrogen oxides during the Chinese economic downturn. Atmos. Chem. Phys. 11 (15), 8171–8188. https://doi.org/10.5194/acp-11-8171-2011.

Lin, K.U.N., Yee-Tak Fong, D., Zhu, B., Karlberg, J., 2006. Environmental factors on the SARS epidemic: air temperature, passage of time and multiplicative effect of hospital infection. Epidemiol. Infect. 134 (2), 223–230. https://doi.org/10.1017/S0950268805005054.

Liu, Y., Gayle, A.A., Wilder-Smith, A., Rocklöv, J., 2020a. The reproductive number of COVID-19 is higher compared to SARS coronavirus. J. Travel Med. 27 (2). https://doi.org/10.1093/jtm/taaa021.

Liu, F., Page, A., Strode, S.A., Yoshida, Y., Choi, S., Zheng, B., ... Joiner, J., 2020b. Abrupt decline in tropospheric nitrogen dioxide over China after the outbreak of COVID-19. Sci. Adv. https://doi.org/10.1126/sciadv.abc2992 eabc2992.

Liu, J., Zhou, J., Yao, J., Zhang, X., Li, L., Xu, X., ... Zhang, K., 2020c. Impact of meteorological factors on the COVID-19 transmission: a multi-city study in China. Sci. Total Environ. 726, 138513. https://doi.org/10.1016/j.scitotenv.2020.138513.

Lolli, S., Chen, Y.-C., Wang, S.-H., Vivone, G., 2020. Impact of meteorological conditions and air pollution on COVID-19 pandemic transmission in Italy. Sci. Rep. 10 (1), 16213. https://doi.org/10.1038/s41598-020-73197-8.

Ma, Y., Zhao, Y., Liu, J., He, X., Wang, B., Fu, S., ... Luo, B., 2020. Effects of temperature variation and humidity on the death of COVID-19 in Wuhan, China. Sci. Total Environ. 724, 138226. https://doi.org/10.1016/j.scitotenv.2020.138226.

Menne, M. J., Durre, I., Korzeniewski, B., McNeal, S., Thomas, K., Yin, X., . . . Houston, T. G. (2012a). Global Historical Climatology Network - Daily (GHCN-Daily). 3.20. https://doi.org/10.7289/V5D21VHZ.

Menne, M.J., Durre, I., Vose, R.S., Gleason, B.E., Houston, T.G., 2012b. An overview of the global historical climatology network-daily database. J. Atmos. Ocean. Technol. 29 (7), 897–910.
NRC, 2001. Climate Influences on Specific Diseases *Under the Weather: Climate, Ecosystems, and Infectious Disease*. National Academies Press, Washington, D.C.
Pan, J., Yao, Y., Liu, Z., Meng, X., Ji, J.S., Qiu, Y., ... Kan, H., 2021. Warmer weather unlikely to reduce the COVID-19 transmission: an ecological study in 202 locations in 8 countries. Sci. Total Environ. 753, 142272. https://doi.org/10.1016/j.scitotenv.2020.142272.
Prata, D.N., Rodrigues, W., Bermejo, P.H., 2020. Temperature significantly changes COVID-19 transmission in (sub)tropical cities of Brazil. Sci. Total Environ. 729, 138862. https://doi.org/10.1016/j.scitotenv.2020.138862.
Sajadi, M.M., Habibzadeh, P., Vintzileos, A., Shokouhi, S., Miralles-Wilhelm, F., Amoroso, A., 2020. Temperature, humidity, and latitude analysis to estimate potential spread and seasonality of coronavirus disease 2019 (COVID-19). JAMA Netw. Open 3 (6), e2011834. https://doi.org/10.1001/jamanetworkopen.2020.11834.
Seo, J.H., Jeon, H.W., Sung, U.J., Sohn, J.-R., 2020. Impact of the COVID-19 outbreak on air quality in Korea. Atmosphere 11 (10). https://doi.org/10.3390/atmos11101137.
Shaman, J., Karspeck, A., 2012. Forecasting seasonal outbreaks of influenza. Proc. Natl. Acad. Sci. 109 (50), 20425. https://doi.org/10.1073/pnas.1208772109.
Shaman, J., Pitzer, V.E., Viboud, C., Grenfell, B.T., Lipsitch, M., 2010. Absolute humidity and the seasonal onset of influenza in the continental United States. PLoS Biol. 8 (2), e1000316. https://doi.org/10.1371/journal.pbio.1000316.
Sheehan, P.E., Bowman, F.M., 2001. Estimated effects of temperature on secondary organic aerosol concentrations. Environ. Sci. Technol. 35 (11), 2129–2135. https://doi.org/10.1021/es001547g.
Shi, X., Brasseur, G.P., 2020. The response in air quality to the reduction of Chinese economic activities during the COVID-19 outbreak. Geophys. Res. Lett. 47 (11). https://doi.org/10.1029/2020GL088070 e2020GL088070.
Skamarock, W.C., Klemp, J.B., 2008. A time-split nonhydrostatic atmospheric model for weather research and forecasting applications. J. Comput. Phys. 227 (7), 3465–3485. https://doi.org/10.1016/j.jcp.2007.01.037.
Stockwell, W.R., Kirchner, F., Kuhn, M., Seefeld, S., 1997. A new mechanism for regional atmospheric chemistry modeling. J. Geophys. Res.-Atmos. 102 (D22), 25847–25879. https://doi.org/10.1029/97JD00849.
Su, T., Li, Z., Zheng, Y., Luan, Q., Guo, J., 2020. Abnormally shallow boundary layer associated with severe air pollution during the COVID-19 lockdown in China. Geophys. Res. Lett. 47 (20). https://doi.org/10.1029/2020GL090041 e2020GL090041.
Sulaymon, I.D., Zhang, Y., Hopke, P.K., Zhang, Y., Hua, J., Mei, X., 2021. COVID-19 pandemic in Wuhan: ambient air quality and the relationships between criteria air pollutants and meteorological variables before, during, and after lockdown. Atmos. Res. 250, 105362. https://doi.org/10.1016/j.atmosres.2020.105362.
Tamerius, J., Nelson Martha, I., Zhou Steven, Z., Viboud, C., Miller Mark, A., Alonso Wladimir, J., 2011. Global influenza seasonality: reconciling patterns across temperate and tropical regions. Environ. Health Perspect. 119 (4), 439–445. https://doi.org/10.1289/ehp.1002383.
Tobías, A., Molina, T., 2020. Is temperature reducing the transmission of COVID-19 ? Environ. Res. 186, 109553. https://doi.org/10.1016/j.envres.2020.109553.
Tosepu, R., Gunawan, J., Effendy, D.S., Ahmad, L.O.A.I., Lestari, H., Bahar, H., Asfian, P., 2020. Correlation between weather and Covid-19 pandemic in Jakarta, Indonesia. Sci. Total Environ. 725, 138436. https://doi.org/10.1016/j.scitotenv.2020.138436.
Wang, P., Chen, K., Zhu, S., Wang, P., Zhang, H., 2020a. Severe air pollution events not avoided by reduced anthropogenic activities during COVID-19 outbreak. Resour. Conserv. Recycl. 158, 104814. https://doi.org/10.1016/j.resconrec.2020.104814.
Wang, J., Tang, K., Feng, K., & Weifeng, L. (2020b). High temperature and high humidity reduce the transmission of COVID-19. SSRN. doi:https://doi.org/10.2139/ssrn.3551767.
Xu, R., Rahmandad, H., Gupta, M., DiGennaro, C., Ghaffarzadegan, N., Amini, H., Jalali, M.S., 2020. The modest impact of weather and air pollution on COVID-19 transmission. medRxiv https://doi.org/10.1101/2020.05.05.20092627 2020.2005.2005.20092627.
Yang, Y., Ren, L., Li, H., Wang, H., Wang, P., Chen, L., ... Liao, H., 2020. Fast climate responses to aerosol emission reductions during the COVID-19 pandemic. Geophys. Res. Lett. 47 (19). https://doi.org/10.1029/2020GL089788 e2020GL089788.
Yao, Y., Pan, J., Liu, Z., Meng, X., Wang, W., Kan, H., Wang, W., 2020. No association of COVID-19 transmission with temperature or UV radiation in Chinese cities. Eur. Respir. J. 55 (5), 2000517. https://doi.org/10.1183/13993003.00517-2020.
Zhang, B., Wang, Y., Hao, J., 2015a. Simulating aerosol–radiation–cloud feedbacks on meteorology and air quality over eastern China under severe haze conditions in winter. Atmos. Chem. Phys. 15 (5), 2387–2404. https://doi.org/10.5194/acp-15-2387-2015.
Zhang, L., Wang, T., Lv, M., Zhang, Q., 2015b. On the severe haze in Beijing during January 2013: unraveling the effects of meteorological anomalies with WRF-Chem. Atmos. Environ. 104, 11–21. https://doi.org/10.1016/j.atmosenv.2015.01.001.
Zhang, Z., Xue, T., Jin, X., 2020. Effects of meteorological conditions and air pollution on COVID-19 transmission: evidence from 219 Chinese cities. Sci. Total Environ. 741, 140244. https://doi.org/10.1016/j.scitotenv.2020.140244.
Zhao, N., Wang, G., Li, G., Lang, J., Zhang, H., 2020. Air pollution episodes during the COVID-19 outbreak in the Beijing–Tianjin–Hebei region of China: an insight into the transport pathways and source distribution. Environ. Pollut. 267, 115617. https://doi.org/10.1016/j.envpol.2020.115617.